CO_2 Reduction

Deutsche Ausgabe: DOI: 10.1002/ange.201601582
Internationale Ausgabe: DOI: 10.1002/anie.201601582

Tailoring Copper Nanocrystals towards C_2 Products in Electrochemical CO_2 Reduction

*Anna Loiudice, Peter Lobaccaro, Esmail A. Kamali, Timothy Thao, Brandon H. Huang, Joel W. Ager, and Raffaella Buonsanti**

Abstract: *Favoring the CO_2 reduction reaction (CO2RR) over the hydrogen evolution reaction and controlling the selectivity towards multicarbon products are currently major scientific challenges in sustainable energy research. It is known that the morphology of the catalyst can modulate catalytic activity and selectivity, yet this remains a relatively underexplored area in electrochemical CO_2 reduction. Here, we exploit the material tunability afforded by colloidal chemistry to establish unambiguous structure/property relations between Cu nanocrystals and their behavior as electrocatalysts for CO_2 reduction. Our study reveals a non-monotonic size-dependence of the selectivity in cube-shaped copper nanocrystals. Among 24 nm, 44 nm and 63 nm cubes tested, the cubes with 44 nm edge length exhibited the highest selectivity towards CO2RR (80 %) and faradaic efficiency for ethylene (41 %). Statistical analysis of the surface atom density suggests the key role played by edge sites in CO2RR.*

Converting carbon dioxide into useful chemicals through an electrochemical process represents a promising path towards establishing a carbon-neutral cycle.[1] High energy density multicarbon products, such as hydrocarbons and alcohols, are much sought after as potential sustainable fuels.[1] Copper is the only metal electrocatalyst with the ability to form substantial amounts of hydrocarbons at the moment.[2] Yet, its efficiency and selectivity are still too low to allow practical implementation of this technology.[1,2] Previous work has shown that the product selectivity depends on the Cu structure.[3–13] For example, Cu (100) increases the selectivity for ethylene while methane is the main hydrocarbon product on Cu (111).[9–12] Recently it has been shown that the selectivity for ethylene can be further increased by utilizing Cu cubes, with around 100 nm edge length, which predominantly show the (100) facets, and nearly completely suppress methane generation.[7] While the (100) surface in single crystals is the most selective for ethylene, it still produces a significant amount of methane.[9–12] The increase of the ethylene yield in the cubes was hypothesized to stem from the convolution of a high density of ethylene-selective active sites, yet to be identified, and local pH changes.[7] Unlike the change in ethylene, the production rate of hydrogen on the cubes was not significantly changed from that of polycrystalline copper.[7]

Size-dependent selectivity of spherical Cu catalysts toward CO_2 reduction has been investigated but with conflicting results.[3,4] Manthiram et al. reported enhanced electrochemical methanation with well dispersed 7 nm Cu nanoparticles compared to Cu foil.[4] In contrast, Reske et al. found that Cu nanoparticles smaller than 30 nm produced hydrogen as the main product.[3] Unambiguous conclusions cannot be made as these catalysts were synthesized by different approaches and different measurement conditions were employed.[3,4]

Here, we explore the effect of both size and shape of Cu nanocrystals (NCs) on their CO_2 electroreduction activity and product selectivity. Two different sizes of Cu NC spheres (7.5 nm and 27 nm) and three different sizes of Cu NC cubes (24 nm, 44 nm, and 63 nm) were synthesized by the same colloidal chemistry-based method. Within the same morphology, smaller NCs exhibited higher activity; however overall, the cube-shaped NCs were more intrinsically active than the spheres, as discussed below. An unexpected non-monotonic selectivity trend was observed, with an 80 % selectivity for carbon products observed, 50 % of which corresponded to ethylene, for the Cu NC cubes with 44 nm side length.

Figure 1 A–E shows the transmission electron microscopy (TEM) images of the synthesized Cu NC cubes and spheres which exhibit uniformity of size and shape (Figure S1 in the Supporting Information). Figure 1 F compares the typical X-ray diffraction (XRD) patterns for the as-synthesized Cu NC cubes and spheres. In the Cu cubes, the (200) peak is more pronounced than that of the bulk fcc Cu reference, which indicates the predominance of {100} facets.

The Cu NC catalysts were spin-coated on glassy carbon, which served as the working-electrode in a three-electrode setup containing CO_2-saturated 0.1 M potassium bicarbonate as the electrolyte. Figure 2 reports the current densities, normalized by the electrochemically active surface area

[*] Dr. A. Loiudice, E. A. Kamali, Prof. R. Buonsanti
Department of Chemical Sciences and Engineering
École Polytechnique Fédérale de Lausanne
1950 Sion (Switzerland)
E-mail: raffaella.buonsanti@epfl.ch
P. Lobaccaro, Dr. J. W. Ager
Joint Center for Artificial Photosynthesis
Lawrence Berkeley National Laboratory
Berkeley, CA 94720 (USA)
P. Lobaccaro, B. H. Huang
Department of Chemical and Biomolecular Engineering
University of California, Berkeley
Berkeley, CA 94720 (USA)
T. Thao, Dr. J. W. Ager
Department of Materials Science and Engineering
University of California
Berkeley, CA 94720 (USA)
Supporting information and the ORCID identification number(s) for the author(s) of this article can be found under http://dx.doi.org/10.1002/anie.201601582.

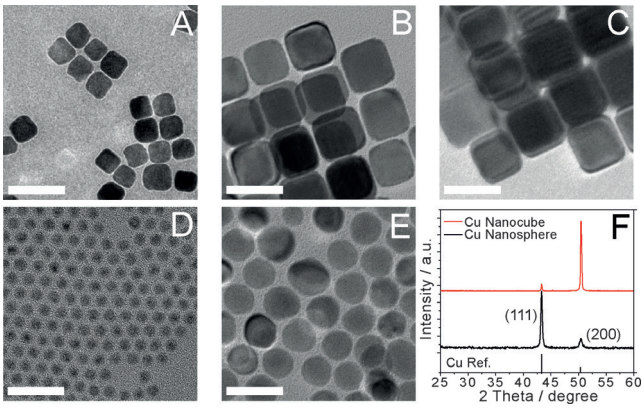

Figure 1. A–C) TEM images of Cu cubes with an average edge length of 24, 44, 63 nm, respectively; D–E) TEM images of Cu spheres with an average diameter of 7.5 and 27 nm, respectively. Scale bar 50 nm. F) Typical XRD patterns of the Cu spheres (black line) and Cu cubes (red line).

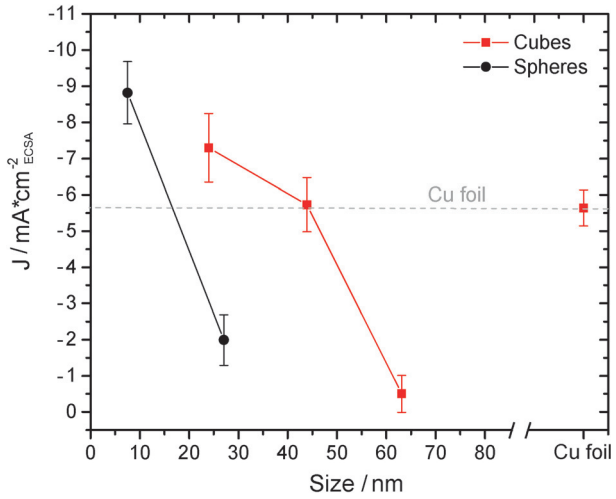

Figure 2. Current density at −1.1 V vs. RHE are plotted against the size of the Cu NC catalysts. The complete linear sweep voltammograms are reported in Figure S3. The error bars indicate the standard deviation of five independent measurements. High purity Cu foil was used as a control-working electrode and showed current density comparable to Kuhl et al.[2]

(ECSA), corresponding to the different Cu catalysts at −1.1 V vs. RHE. When comparing electrodes with different areas, it is important to know their relative number of active surface sites, as a larger surface area can lead to a larger apparent activity, without fundamentally changing the underlying catalytic ability of the material. Among the different techniques, we chose to normalize the current density by the ECSA measured using the Randles-Sevcik equation (Figures S2). A discussion about different methods to estimate surface area is reported in Figure S3 and Table S1. Figure 2 evidences that the smallest spheres (7.5 nm) and the cubes of 24 nm and 44 nm exhibited larger current density than Cu foil. Instead, the 27 nm spheres and the 63 nm cubes were less active (lower current density) than Cu foil. Within the particles of the same shape, there is a monotonic size-dependent trend, where smaller NCs are more active than bigger ones. Such trends are similar to what was observed by Reske et al. for their Cu spheres.[3] Interestingly, the size-dependence does not hold when Cu cubes and Cu spheres are compared, with the 44 nm cubes showing a higher current density than the 27 nm spheres, indicating a higher intrinsic activity for the cubes.

To gain insights into the CO2RR and the competing hydrogen evolution reaction (HER) of the synthesized Cu NCs, faradaic efficiency (FE) measurements were performed in an electrochemical flow cell (Figure S4) and at −1.1 V vs. RHE, where HER is less favorable (Figure S5). Herein, the focus is on the size-dependent activity of the cubes, as it has not been investigated before. Figure 3 reports the faradaic

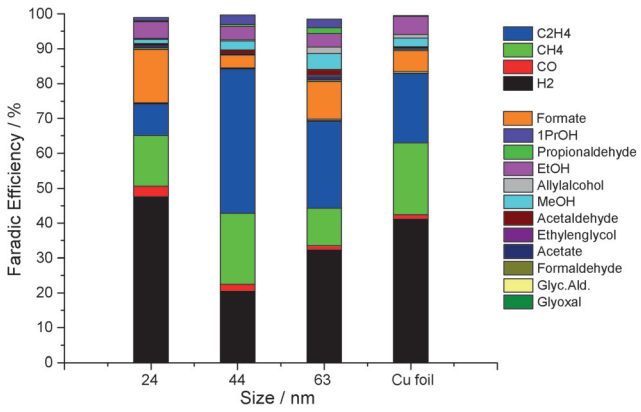

Figure 3. Bar graph reporting the faradaic efficiencies for each product in the different size of Cu NC cubes and in the Cu foil at −1.1 V vs. RHE. The glassy carbon signal has been subtracted.

efficiency for each product detected by gas and liquid chromatography for the various Cu cubes compared to Cu foil. Each data point represents the average of three independent measurements. For comparison, the FE measurements relative to the spheres are reported in Figure S6 and Table S3. Stable currents were measured during the one hour electrolysis (Figure S7). Importantly, scanning electron microscopy confirmed that the morphology of the Cu NC cubes was preserved during electrolysis (Figure S8).

When aiming to maximize the performance of CO2RR catalysts, higher selectivity for CO2RR over HER and for higher hydrocarbons are much sought after. Thus, we have decided to focus on the selectivity for CO2RR over HER (FE_{CO2RR}), the faradaic efficiency for ethylene (FE_{C2H4}) and the selectivity for ethylene versus methane (C_2H_4/CH_4) as figures of merit to discuss the catalytic performance of our Cu NC cubes. Table 1 summarizes the results. First, we note that the smaller cubes show equal activity for HER and CO2RR ($FE_{CO2RR} = 50\,\%$), with C1 products, and specifically methane and formate being the major carbonaceous species ($C_2H_4/CH_4 = 0.63$, Table S3). As the size of the cubes increases, the three figures of merit improve. The cubes with 44 nm edge length exhibited the best performance with the highest selectivity toward CO2RR ($FE_{CO2RR} = 80\,\%$) and with ethylene as the major reduction product ($FE_{C2H4} = 41\,\%$, $C_2H_4/$

Table 1: Figures of merit to describe the CO2RR catalytic behavior of the Cu NCs cubes compared with Cu foil.

Size [nm]	FE_{CO2RR} [%][a]	FE_{C2H4} [%]	C_2H_4/CH_4[b]
24	43	9	0.63
44	80	41	2.03
63	63	25	2.33
Cu foil	56	20	1

[a] $FE_{CO2RR} = 100 \times FE_{CO2RR}/(FE_{CO2RR} + FE_{HER})$, where FE_{CO2RR} is the sum of the FEs of all the C-products. [b] $C_2H_4/CH_4 = FE_{C2H4}/FE_{CH4}$.

$CH_4 = 2.03$). The largest cubes showed a slight increase in C_2H_4/CH_4; however, the overall CO2RR activity decreased and the ethylene production was lower ($FE_{C2H4} = 25\,\%$).

The surface metal atomic coordination and corresponding surface electronic structure, along with the surface pH, have been identified as crucial parameters to explain the CO2RR selectivity in nanostructured and NC-based Cu electrodes.[3,7,11,13–16] In agreement with Reske et al., we exclude a significant role of local pH changes to explain the selectivity changes in our catalysts.[3] In fact, in the Cu NC cubes with 24 nm edge length, which produce larger current densities, we would expect the pH increase to lead to lower hydrogen production, which is not the case.[3,7] Instead, the analysis of the active sites (plane-, edge- and corner-type) on the surface aids better to rationalize the non-monotonic nature of the selectivity trend.[3,17,18]

As discussed in the introduction, the exposed crystalline planes have an influence on the CO2RR selectivity, with the (100) and the (111) surfaces favoring ethylene and methane formation, respectively.[7,9–12] In the Cu NC cubes, the collected XRD patterns indicate that the {100} facets predominate on the surface. We used a simple model to derive the statistics of surface atoms for Cu NC cubes (Figure 4 and Table S4). As the NC size increases, the relative number of atoms on the corners and on the edges decreases while the number on plane increases; thus, we move towards a surface configuration closer to one single crystal with all the surface atoms laying on (100) planes. The sizes of the smaller Cu NC cubes (edge length ≤ 24 nm) is on the upper end of the size range studied by Reske et al.[3] Based on their findings, the higher density of low-coordinated sites (corners, steps and kinks) might account for their high activity (higher current density) and the HER selectivity compared to the other samples. The trend of the active sites with the size suggests that the unique reactivity of the 44 nm Cu NC cubes derives from an optimal balance between plane- and edge- sites. Thus, we highlight the importance of atoms on the edges as CO2RR and ethylene-selective active sites in the Cu NC cubes. The role of edge sites has been longer recognized in catalysis.[18,19] Furthermore, this hypothesis is consistent with the size-dependence studies on Au NCs as CO_2 electroreduction catalysts.[18] Using density functional theory, edge sites were identified as key sites which facilitate the adsorption and stabilization of CO2RR reaction intermediates (i.e. COOH*) and inhibits HER. The dominance of such sites on 8 nm Au NCs made them more active and selective for CO2RR than 4, 6, 10 nm ones.[18]

Catalysts which are selective for CO2RR and favor C–C coupling are much sought after. Through a careful investigation of Cu NCs with different sizes and shapes produced by the same colloidal approach, we confirm the increased selectivity for ethylene on Cu NC cubes, in agreement with previous works.[7] In addition, we reveal a unique size-dependent selectivity with the highest selectivity for CO2RR and C_2 products found in 44 nm Cu cubes. This result emphasizes that an optimal ratio of edge sites over (100) plane-sites ($N_{edge}/N_{100} = 0.025$ for $d = 44$ nm) is crucial to maximize CO2RR and ethylene selectivity. Our work represents a step further towards ultimately identifying which structural parameters in CO_2 reduction electrocatalysts control the selectivity towards multicarbon products. Future work on ultrathin structures and nanoframes, which possess a high density of edge atoms, might be desirable to further improve the selectivity towards CO2RR and towards C–C coupling. Considering the possibility of colloidal chemistry to access a wide compositional space, this work is foundational in demonstrating the use of atomically defined colloidal NCs as a materials platform for advancing CO_2 reduction.[20]

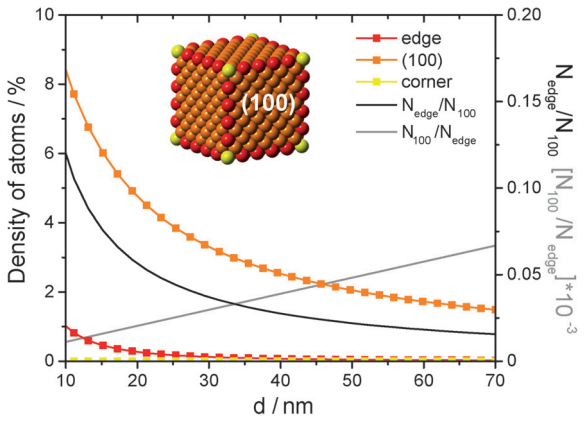

Figure 4. On the left axis: Density of adsorption sites in Cu NC cubes reported versus the edge length (d). On the right axis: trend of N_{edge}/N_{100} and N_{100}/N_{edge} versus d, where N_{edge} is the number of atoms at the edge and N_{100} is the number of atoms on the (100) plane.

Experimental Section

NCs synthesis: Cu NCs spheres and cubes were synthesized according to modifications of literature methods.[21] For the synthesis of Cu cubes of 24 nm, CuBr (3 mmol) and TOPO (25 mmol) were dissolved into oleylamine (10 mL) in a three-necked flask by vigorous magnetic stirring at 80 °C for 15 min. Then the resulting solution was heated up to 210 °C quickly and refluxed at this temperature for 1 h before cooling down to room temperature naturally. In order to obtain Cu nanocubes with a larger edge length (44 nm), the content of TOPO was reduced to 7.5 mmol and the content of CuBr to 1.5 mmol dissolved in 35 mL of oleylamine. Then the resulting solution was heated up to 220 °C quickly and refluxed at this temperature for 1 h. In order to obtain Cu nanocubes with a larger edge length (63 nm), the content of TOPO was reduced to 2.5 mmol, while the temperature and the aging time was increased to 260 °C and 2.5 h, respectively. Cu NCs spheres were obtained by following similar procedure. For the synthesis of Cu spheres of 27 nm, oleylamine (35 mL) and CuBr (3 mmol) were mixed in a three-necked flask by strong magnetic stirring at 80 °C for 15 min, then TOP (6 mmol) was injected into the obtained green solution, which immediately became colorless. After

an additional stirring at 80 °C for 5 min, the mixed solution was heated up to 260 °C quickly and kept at this temperature for 3 h before cooling down to room temperature naturally. Excess hexane was added to the bright reddish solution, and the Cu cubes were precipitated out by centrifugation. The volume of hexane in which the nanocrystals were suspended was adjusted in order to have a concentration of 1.5 mg mL^{-1} for each solution.

Electrochemical CO2RR experiments: Electrochemical measurements were carried out using a Biologic SP-300 potentiostat. For gas product analysis, a gas chromatograph (SRI instruments) was used. The liquid products were collected from the cathode and anode chambers after electrolysis and analyzed by high-performance liquid chromatography (HPLC) on an UltiMate 3000 instrument from Thermo Scientific. More detailed experimental procedures are reported in the Supporting Information.

Acknowledgements

We thank Tracy Mattox, at the Molecular Foundry, for elemental analysis of the samples by ICP-AES and Dr. Kendra Kuhl and Dr. Etosha Cave for helpful discussions. The synthetic development and material integration was supported by Laboratory Directed Research and Development (LDRD) funding from Berkeley Lab, provided by the Director, Office of Science, of the U.S. Department of Energy under Contract No. DE-AC02-05CH11231. Electrochemical measurements and product analysis were supported by the Joint Center for Artificial Photosynthesis, a DOE Energy Innovation Hub, supported through the Office of Science of the U.S. Department of Energy under Award Number DE-SC0004993. Faradaic efficiency measurements were supported by the California Energy Commission under agreement 500-11-023. Work at the Molecular Foundry was supported by the Office of Science, Office of Basic Energy Sciences, of the U.S. Department of Energy under Contract No. DE-AC02-05CH11231. B. H. acknowledges the California Energy Corps program for finalncial support.

Keywords: colloidal chemistry · electrochemical CO_2 reduction · nanocrystals · nanocubes · selectivity

How to cite: *Angew. Chem. Int. Ed.* **2016**, *55*, 5789–5792
Angew. Chem. **2016**, *128*, 5883–5886

[1] a) C. Graves, S. D. Ebbesen, M. Mogensen, K. S. Lackner, *Renewable Sustainable Energy Rev.* **2011**, *15*, 1–23; b) X. Lim, *Nature* **2015**, *526*, 628–630.
[2] K. P. Kuhl, E. R. Cave, D. N. Abram, T. F. Jaramillo, *Energy Environ. Sci.* **2012**, *5*, 7050–7059.
[3] R. Reske, H. Mistry, F. Behafarid, B. R. Cuenya, P. Strasser, *J. Am. Chem. Soc.* **2014**, *136*, 6978–6986.
[4] K. Manthiram, B. J. Beberwyck, A. P. Alivisatos, *J. Am. Chem. Soc.* **2014**, *136*, 13319–13325.
[5] W. Tang, A. A. Peterson, A. S. Varela, Z. P. Jovanov, L. Bech, W. J. Durand, S. Dahl, J. K. Norskov, I. Chorkendorff, *Phys. Chem. Chem. Phys.* **2012**, *14*, 76–81.
[6] C. W. Li, M. W. Kanan, *J. Am. Chem. Soc.* **2012**, *134*, 7231–7234.
[7] F. S. Roberts, K. P. Kuhl, A. Nilsson, *Angew. Chem. Int. Ed.* **2015**, *54*, 5179–5182; *Angew. Chem.* **2015**, *127*, 5268–5271.
[8] C. S. Chen, A. D. Handoko, J. H. Wan, L. Ma, D. Ren, B. S. Yeo, *Catal. Sci. Technol.* **2015**, *5*, 161–168.
[9] Y. Hori, I. Takahashi, O. Koga, N. Hoshi, *J. Mol. Catal. A* **2003**, *199*, 39–47.
[10] K. J. P. Schouten, E. Perez Gallent, M. T. M. Koper, *ACS Catal.* **2013**, *3*, 1292–1295.
[11] K. J. P. Schouten, Z. Qin, E. Perez Gallent, M. T. M. Koper, *J. Am. Chem. Soc.* **2012**, *134*, 9864–9867.
[12] K. J. P. Schouten, Y. Kwon, C. J. M. van der Ham, Z. Qin, M. T. M. Koper, *Chem. Sci.* **2011**, *2*, 1902–1909.
[13] R. Kortlever, J. Shen, K. J. P. Schouten, F. Calle-Vallejo, M. T. M. Koper, *J. Phys. Chem. Lett.* **2015**, *6*, 4073–4082.
[14] R. Kas, R. Kurtlever, H. Yilmaz, M. T. M. Koper, G. Mul, *ChemElectroChem* **2015**, *2*, 354–358.
[15] K. J. P. Schouten, E. Perez Gallent, M. T. M. Koper, *J. Electroanal. Chem.* **2014**, *716*, 53–57.
[16] W. J. Durand, A. A. Peterson, F. Studt, F. Abild-Pedersen, J. K. Norskov, *Surf. Sci.* **2011**, *605*, 1354–1359.
[17] a) M. Crespo-Quesada, A. Yarulin, M. Jin, Y. Xia, L. Kiwi-Minsker, *J. Am. Chem. Soc.* **2011**, *133*, 12787–12794; b) T. Chen, S. Chen, Y. Zhang, Y. Qi, Y. Zhao, W. Xu, J. Zeng, *Angew. Chem. Int. Ed.* **2016**, *55*, 1839–1843; *Angew. Chem.* **2016**, *128*, 1871–1875.
[18] a) W. Zhu, R. Michalsky, O. Metin, H. Lv, S. Guo, C. J. Wright, X. Sun, A. A. Peterson, S. Sun, *J. Am. Chem. Soc.* **2013**, *135*, 16833–16836; b) W. Zhu, Y.-J. Zhang, H. Lv, Q. Li, R. Michalsky, A. A. Peterson, S. Sun, *J. Am. Chem. Soc.* **2014**, *136*, 16132–16135; c) A. A. Peterson, *ECS Trans.* **2015**, *66*, 41–52.
[19] a) B. Ni, X. Wang, *Adv. Sci.* **2015**, *2*, 1500085; b) T. F. Jaramillo, K. P. Jørgensen, J. Bonde, J. H. Nielsen, S. Horch, I. Chorkendorff, *Science* **2007**, *317*, 100–102; c) J. Kibsgaard, Z. Chen, B. N. Reinecke, T. F. Jaramillo, *Nat. Mater.* **2012**, *11*, 963–969.
[20] M. V. Kovalenko, L. Manna, A. Cabot, Z. Hens, D. V. Talapin, C. R. Kagan, V. I. Klimov, A. L. Rogach, P. Reiss, D. J. Milliron, P. Guyot-Sionnest, G. Konstantatos, W. J. Parak, T. Hyeon, B. A. Korgel, C. B. Murray, W. Heiss, *ACS Nano* **2015**, *9*, 1012–1057.
[21] H. Guo, Y. Chen, M. B. Cortie, X. Liu, Q. Xie, X. Wang, D.-L. Peng, *J. Phys. Chem. C* **2014**, *118*, 9801–9808.

Received: February 14, 2016
Published online: April 5, 2016

